Spinel Ferrites for Supercapacitor Applications

भारतीय विज्ञान शिक्षा एवं अनुसंधान संस्थान, पुणे

INDIAN INSTITUTE OF SCIENCE EDUCATION AND RESEARCH (IISER), PUNE

(An Autonomous Institution, Ministry of Human Resource Development, Govt. of India)

Dr. Homi Bhabha Road, Pashan, Pune 4110 008

5th year Master of Science Thesis

Name: Amit Choudhary

Registration no. : 20141151

Supervisor: Prof. P. A. Joy, NCL Pune

TAC expert: Prof. Muhammed Musthafa O. T., IISER Pune

Duration: June, 2018 - March, 2019

सीएसआईआर - राष्ट्रीय रासायनिक प्रयोगशाला
(वैज्ञानिक तथा औद्योगिक अनुसंधान परिषद)
डॉ. होमी भाभा मार्ग, पुणे - 411 008, भारत

CSIR - NATIONAL CHEMICAL LABORATORY
(Council of Scientific & Industrial Research)
Dr. Homi Bhabha Road, Pune - 411 008, India

Certificate

This is to certify that this dissertation entitled **"Spinel Ferrites for Supercapacitor Applications"** towards the partial fulfillment of the BS-MS dual degree programme at the Indian Institute of Science Education and Research, Pune, represents study and work carried out by **Mr. Amit Choudhary** at CSIR-National Chemical Laboratory, Pune under the supervision of **Dr. P. A. Joy**, Chief Scientist, Physical and Materials Chemistry Division, CSIR-NCL, Pune during the academic year 2018-2019.

Date: March 29, 2019

Dr. P. A. Joy
Chief Scientist
Physical and Materials Chemistry Division
Email: pa.joy@ncl.res.in

Communication Channels

☎
NCL Level DID : 2590
NCL Board No. : +91-20-25902000
EPABX : +91-20-25893300
: +91-20-25893400

FAX
Director's Office : +91-20-25902601
COA's Office : +91-20-25902660
SPO's Office : +91-20-25902664

WEBSITE
www.ncl-india.org

Declaration

I hereby declare that the matter embodied in the report entitled "Spinel **Ferrites for Supercapacitor Applications**" are the results of the work carried out by me at the Department of Physical and Material Chemistry Division, CSIR-NCL, Pune, under the supervision of **Dr. P. A. Joy** and the same has not been submitted elsewhere for any other degree.

Amit

Date: March 29, 2019

Amit Choudhary

Acknowledgement

It is a great pleasure for me to express my gratitude and heart full thanks to each and everyone, who have helped me, directly or indirectly to complete this work.

My deepest and heartiest thanks goes to my research supervisor Dr. P.A. Joy, Chief Scientist, Physical and Materials Chemistry Division, CSIR-NCL, Pune, who has given me a wonderful exposure about research and his dedication, sincerity in research have been inspired me more to complete my work with much clarity. I am so blessed to work under his guidance.

I express my immense and sincere gratitude to for providing me an opportunity to work under his guidance and the care, support and healthy suggestion given by him helped me a lot to complete my research work in the given period of time. I am always thankful to him.

It is my privilege to express my gratitude to the TAC member Dr. Muhammed Musthafa, Assistant Professor, IISER Pune, for his suitable suggestions; comments guided me during the testing time of my project. My sincere thanks to him for his timely helps, care and supports on all occasion during my project period.

My grateful greets to Dr. Ashwini Kumar Nangia, Director of CSIR-NCL, Pune, for the infrastructure and the facilities to carry out my research work in the prestigious laboratory. I would also like to express my gratitude to Dr. Ramsundar, Dr. Manjunath, Mr. Mohan, Mr. Arun and Ms. Anupriya, for helping me to complete my laboratory work successfully.

.

Contents

Chapter1

Introduction

1.1 Material Science

Material Science is an interdisciplinary subject that includes chemistry, physics, biology, crystallography etc. with engineering for technological applications. With the outstanding growth in science and technology, different material have been invented pertaining to different applications such as sensors, actuators etc [1]. Materials have been found with different physical and chemical properties and these properties in turn depend on the structure of the parent material. By understanding this structure- properties relationship new material with enhanced properties can be developed.

In the recent years much attention has been given to composite material and on the optimization of their processing to get desired properties. Composite materials are synthesized by combining two or more materials and their specific composition generates properties different form individual ones.

1.1.1 Ferrites

Ferrites are ferrimagnetic ceramic oxides having Fe_2O_3 as its main component. Ferrites are a type of magnetic materials that show both electrical and magnetic properties [2].Ferrites are ionic in nature and have dielectric losses, low eddy current and high electrical resistivity which makes them ideal candidates in field of technological applications.

1.1.2 Classification of ferrites

Ferrites can be classified based on the magnetic properties and based on the crystal structure [3].

Based on the magnetic properties ferrites are of mainly two types- Soft Ferrites and Hard ferrites.

Based on the crystal structure ferrites are of four types mainly- Spinel, Ortho, Garnet and Hexaferrites.

1.1.3 Spinel Oxides

Spinel type oxide is a class of material that crystallizes in a FCC (face centered cubic) structure system with general formula AB_2O_4 [4]. In general, A and B are divalent and trivalent cations respectively. If these systems have Fe as major component they are called as ferrites.

1.1.4 Crystal Structure of Spinel Oxides

Spinel type oxides are derived from their general formula, $MgAl_2O_4$ and can be represented by the general formula AB_2O_4. The unit cell of a spinel consists of eight formula units and therefore one can represent it as $8[AB_2O_4]$ or $A_8B_{16}O_{32}$. Within the face centered cubic lattice constructed by 32 oxygen ions there exist two type of interstitial position which can be captured by the metallic cations. There are 64 tetrahedral sites surrounded by 4oxygens and 32 octahedral sites surrounded by 6 oxygens. In spinel structures, 8 out of 64 tetrahedral sites and 16 out of 32 octahedral sites are employed by cations. For better understanding, the unit cell of edge length *a* can be divided into 8 octants with edge length *a*/2. The space group for the spinel ferrites has been identified as Fd3m with the space group number 227 [5].

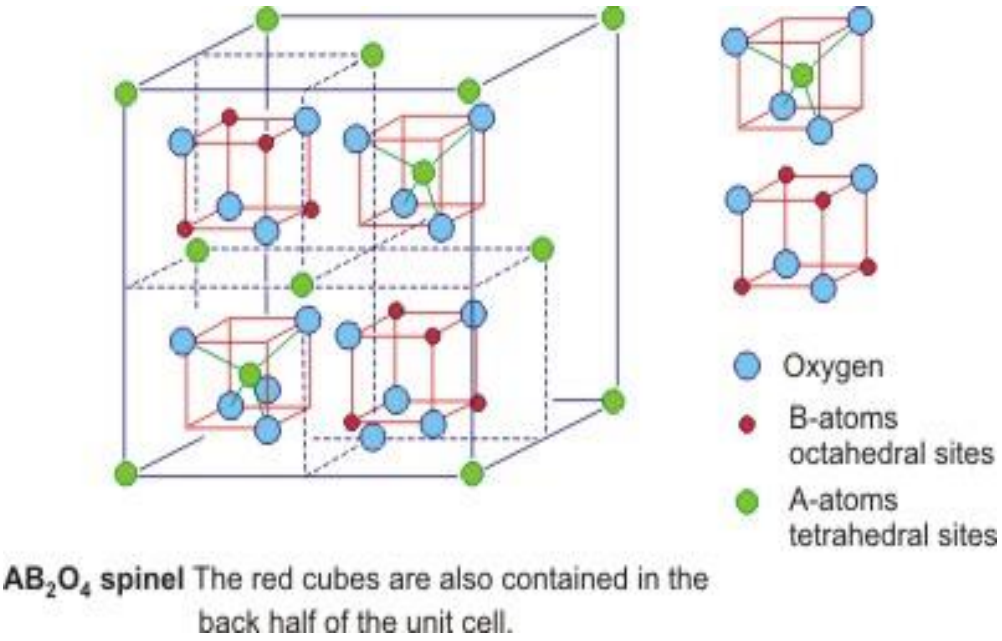

Diagram 1: Cubic spinel oxide crystal structure is shown with atoms occupying their respective sites [6]

Depending upon the occupation and redistribution of the cations in the tetrahedral and octahedral sites, spinels are categorized as normal, inverse and mixed spinel.

Table1: Types of Spinel Oxides and their general formula.

S.No.	Type	General Formula
1	Normal	AB_2O_4
2	Inverse	$B(AB)O_4$
3	Mixed	$A_{1-x}B_x(A_{x/2}B_{1-x/2})O_4$ where $0<x<1$

1.1.5 Applications of Spinel Ferrites

1. In batteries, supercapacitors.
2. Magnetic sensors
3. Pollution Control
4. Transducers
5. Catalysis [7]

1.2 Supercapacitor

1.2.1 Introduction

Amidst the growing demand of efficient, sustainable and clean energy alternative options are being explored other than fossil fuels. Regarding this much attention has been given to supercapacitors to meet energy requirement targets. Supercapacitor incorporates the properties of both batteries and capacitors. Supercapacitors are also known as electrochemical capacitors and have higher charge storage capacity compared to the conventional capacitors [8]. Conventional capacitors consist of two parallel plates separated by insulator. The process of energy storage is non faradic. The energy storage is carried by separation of positive and negative charges.

Supercapacitors have high power and energy storage capabilities. Apart from short charging and discharging time, supercapacitors have long cycle life.

1.2.2 Principle

In supercapacitors energy is stored by polarizing the electrolytic solutions. The charges are separated at electrode electrolyte interface. one layer is formed on the electrode surface and the other is comprised of ions in the electrolyte.

1.2.3 Working

There are two metal electrodes separated by a separator. When the voltage is applied in positive part, it attracts negative ions from the electrolyte and vice versa. This leads to the formation of a layer on both sides of the plate. This phenomenon is called as double layer formation. It is generally accepted that there are two charge storage mechanisms involved in the operation of supercapacitors:

a) electrostatically storing the charges at the interface of capacitor electrode as electric double layer capacitance.

b) faradaically storing the charges at the electrode surface as pseudocapacitance[9].

Electric double layer (EDL) refers to the two charged layers formed at the electrode/electrolyte interfaces and the resulting potential-dependent charge storage ability is ascribed to electric double layer capacitance. Pseudocapacitance arises at the electrode surfaces where the charges are faradaically stored. Stemming from thermodynamic reasons, the faradaic charge transfer process across the electric double layer leads to a special potential-dependent charge accumulation or release phenomenon such that the derivative dq/dV is equivalent to a capacitance. It is manifested by the triangular shape of charge/discharge curves at constant current density and the rectangular shape of cyclic voltammograms for pseudocapacitors.

1.2.4 Classification of Supercapacitors

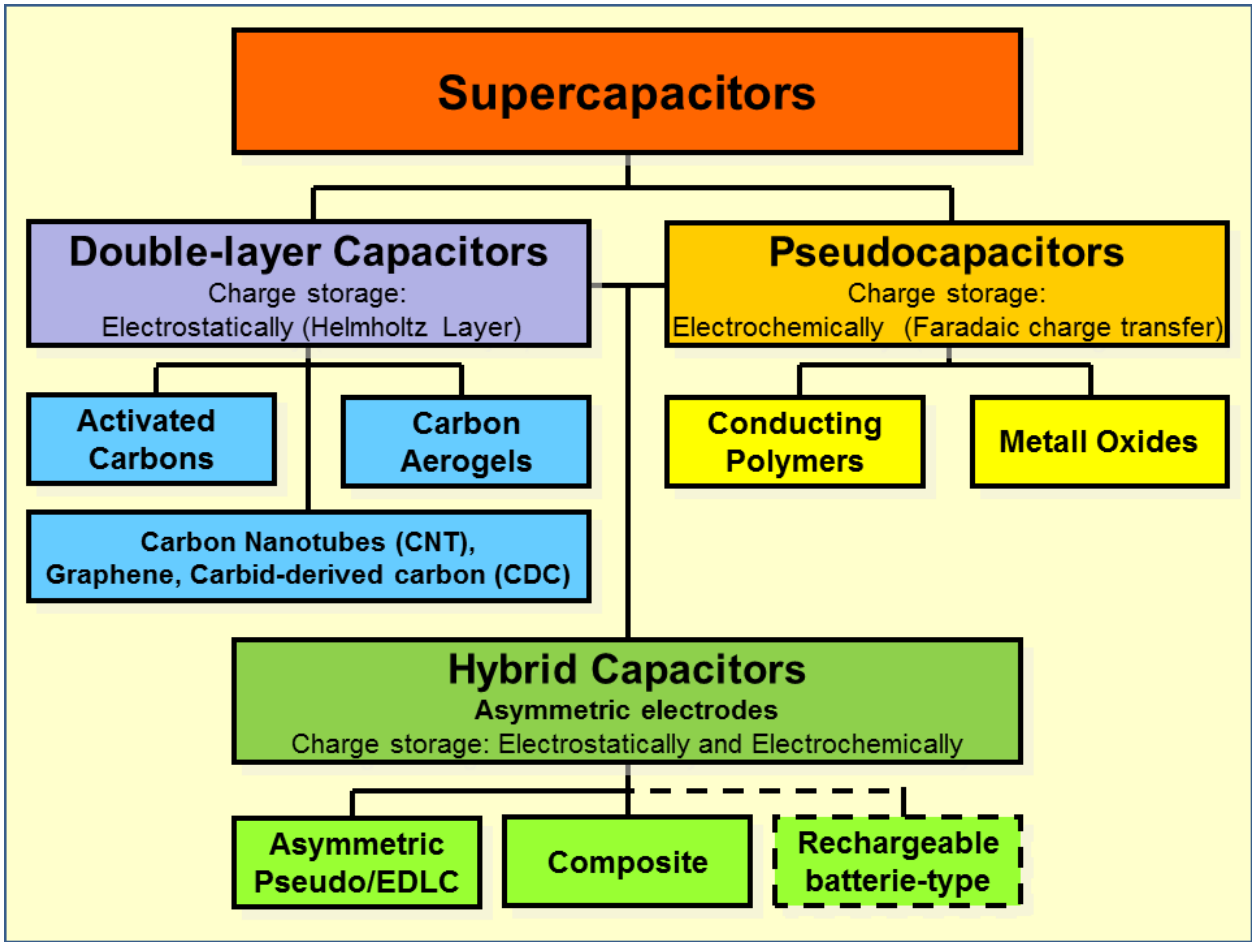

Diagram 2: Tree diagram showing different types of supercapacitor [10]

1.3 Aim of the present study

Recently, several electrode materials are being investigated and researched for their potential use as materials for supercapacitor applications. In this regard much attention has been given to nanosized spinel ferrite materials and their composites. Nanosized particles have high surface area which in turn significantly affect the electrochemical characteristics of the material.

In this study nanosized spinel ferrites are synthesized and electrochemical properties are studied considering them efficient candidates for supercapacitor applications.

The Prime objective of the present study is to synthesize different nanosized spinel ferrites for supercapacitor applications.

Chapter 2

Experimental methods and characterization techniques

2.1 Introduction

Various chemical methods such as coprecipitation, autocombustion, citrate-gel, sol-gel, hydrothermal etc. are used for synthesis of spinel oxide nanoparticles. In the present work autocombustion method was used to synthesize nanostructured spinel ferrites.

2.2 Methods of synthesis

2.2.1 Coprecipitation Method

It is a viable route for synthesis of spinel nanoparticles by using their corresponding metal nitrates, dissolved in distilled water. After precipitating with a precipitating agent either the spinel oxide is directly formed or a precursor is formed which can be calcined to get the desired product. Three major steps are involved in coprecipitation process. Nucleation, growth and agglomeration [8].

2.2.2 AutoCombustion Method

It is a low temperature self sustainable synthesis involving like metal nitares and diffenet oxidizers like glycine, citric acid, tartaric acid etc [1]. The name autocmbustion governs the fact that reaction is spontaneously occuring once ignited. The reaction is exothermic and various gases are evolved during the reaction. In the present study, glycine is used as fuel for autocombustion synthesis. Glycine is a bidendate ligand with carboxylic and amino group which facilitates the binding of these groups to metal ion with strong coordination bonds. In particular, one mole of glycine binds to two moles of metal ions. Flame temperature of the reaction depends upon the fuel to oxidant ratio as well as on amount of glycine.

The complete combustion reaction for the synthesis of spinel compounds can be expressed as the following chemical equation.

$$A(NO_3)_2.3H_2O + 2\ B(NO_3)_2.9H_2O + 4.44\ C_2H_5NO_2 \rightarrow AB_2O_4 + CO_2 + H_2O + N_2$$

In the above equation, 4.44 moles of glycine or 1.48 moles of glycine per metal ion are required for the synthesis of 1 mole of spinel compound. By varying glycine to metal ion ratio, one can tune the size of the crystallite powders [13].

Main advantages of glycine-nitrate autocombustion method are:

1. It is less time consuming and simple single step method.

2. This method is suitable for preparing larger quantities of sample.

3. Crystallite size of ferrites powders can be tune by changing glycine to metal ion ratio.

4. High purity and homogeneity in the particles of ferrite powders can be obtained.

5. The method is applicable for the preparation of almost all spinel ferrite compounds.

In the present study, spinel ferrite powders are synthesized by using this method. Stoichiometric amounts of metal ions are weighed and dissolved in minimum amount of distilled water in a beaker. Calculated amount of glycine corresponding to glycine per metal ion ratio is separately dissolved in minimum amount water and kept for sonication for 15 minutes. After that both the compounds are mixed together and further kept for sonication for 15minutes. This compound is then transferred to a crystalline dish and kept on hot plate for heating at 200^0C. After complete evaporation of water self ignitions happens and fluffy mass of spinel ferrite compound is obtained.

2.3 Characterization techniques

X-ray Diffraction

X-ray diffraction is a characterization technique extensively used in the field of material science. Each crystalline material has its own X-ray diffraction pattern, therefore X-ray diffraction pattern is called as a fingerprint of the crystalline material. X-ray diffraction helps in the analysis of structural aspects of material and to identify the different phases, including impurities and unreacted compounds in a given material. These informations are very useful guidance for the modification of synthesis parameters.

Bragg has derived an equation, which relate wavelength of an incident electromagnetic radiation to the diffraction angle and lattice spacing in a crystalline sample. When a series of X-rays incident on the sample then X-rays are reflected from a pair of parallel planes of atom [13]. If the reflected beams interfere constructively, one observes the intensity maximum at the particular

angle. If θ is the angle of incident rays and if the path difference equal to whole number of wavelength (nλ), and d is perpendicular distance between a pair of crystallite planes then the following relationship can be established between them, known as Bragg's equation.

$$n\lambda = 2d\sin\theta$$

It is well-known in the literature that diffracted peaks obtained from XRD patterns having an extra broadening when the crystallite size is below a certain value (<100 nm) [14]. Hence, average crystallite size(t) can be calculated by measuring the width of the XRD peak, using Scherer's formula given by [17].

$$t=0.9\times\lambda / \beta\times\cos\Theta$$

Where t is average crystallite size, λ is wavelength of Cu K-alpha, β is full width half maximum, Θ is angle of diffraction.

In the present study, XRD patterns of the calcined and sintered powders were recorded on a PANalytical X'pert pro powder X-ray diffraction using Cu-K_α radiation with a wavelength of 1.5405 Å for $K_{\alpha1}$ and 1.5443 Å for $K_{\alpha2}$. The sample was scanned in the 2θ range 10-80 degrees for 1Hour.

Electrochemical characterization

Electrochemical characteristics were studied on a Biologic VMP 300 electrochemical workstation using a three electrode system composed of glassy carbon (working electrode), platinum electrode(counter electrode) and Hg/HgO electrode(reference electrode). The details of electrode preparation, depending on the material have been in the following chapters 3 and 4.

Cyclic Voltammetry (CV) and Galvanostatic charge discharge(GCD) :

Cyclic Voltammetry (CV) technique applies a linearly changed electric potential between reference and working electrodes for three-electrode configurations. The speed of the potential change in mV s^{-1} is designated as the scan rate and the range of potential change is

called the potential window or operating potential. The instantaneous current during the cathodic and anodic sweeps is recorded to characterize the electrochemical reactions involved. The data are plotted as current (I) vs. potential (V).

Galvanostatic Charge Discharge (GCD) technique is the most widely used method for the characterization of SCs under. It is conducted by repetitive charging and discharging of the SC device or the working electrode at a constant current level with or without a dwelling period (a time period between charging and discharging while the peak voltage and normally a plot of the potential (E) vs. time (s) is the output.

From Cyclic Voltammetry (CV) measurements the specific capacitance of the electrode is evaluated as per the following equations,

$$C = \text{Area}/(2*\text{scan rate}*m*\Delta V) \quad \rightarrow (1)$$

Where C is specific capacitance in Farad per gram, Area is the integrated area under the curve from the cyclic voltammetry measurement, m is the weight of the material loaded on the electrode, ΔV is the potential window in volts.

From Galvanostatic Charge Discharge (GCD) measurements specific capacitance of the electrode is evaluated as per the following equation

$$C = I*\Delta t/m*\Delta V \quad \rightarrow (2)$$

Where C is specific capacitance in Farad per gram, I is current in Ampere, Δt is discharge time in seconds, m is the weight of the material loaded on the electrode, ΔV is the potential window in volts for full discharge [15, 16].

Chapter 3

Electrochemical studies on divalent ion substituted spinel ferrites

3.1 Introduction

In the present study spinel ferrites of the form AFe_2O_4 are synthesized where A is divalent metal ion like Cr^{2+}, Mn^{2+}, Ni^{2+}, Cu^{2+}, Zn^{2+} . These divalent metal ions from transition metal group can exhibit multiple oxidation states and form the redox couple which makes them as potential candidates for supercapacitor applications [18]. These divalent metal ions have different number of valence electrons so the objective of the present study is to infer the role of the respective electronic structure of these divalent metal ions affecting electrochemical characteristics.

3.2 Material synthesis

Autocombustion method is employed for the synthesis of nanostructured AFe_2O_4 synthesized where A is divalent metal ion like Cr^{2+}, Mn^{2+}, Ni^{2+}, Cu^{2+}, Zn^{2+}. The Stoichiometric amounts of $Al(NO_3)_2.3H_2O$ and $Fe(NO_3)_3.9H_2O$ are dissolved with glycine(fuel) in minimum amount of DI water in a beaker. The metal ion to glycine mole ratio of 0.5 is taken. The solution is kept into a crystalline dish heated at 250^oC on a hot plate. After complete autocombustion, ash is collected and X-ray diffraction studies are done to confirm the formation of spinel phase.

3.3 Material Characterization

In the present study, XRD patterns of the calcined and sintered powders were recorded on a PANalytical X'pert pro powder X-ray diffraction using Cu-K_α radiation with a wavelength of 1.5405 Å for $K_{\alpha1}$ and 1.5443 Å for $K_{\alpha2}$. The K_β component which is having a wavelength of 1.3922 Å was removed using Ni-β filter. The voltage and current applied for X-ray tube to generate the required wavelength were 30 mA and 40 kV, respectively and the sample was scanned in the 2θ range 10-80 degrees for 1Hour.

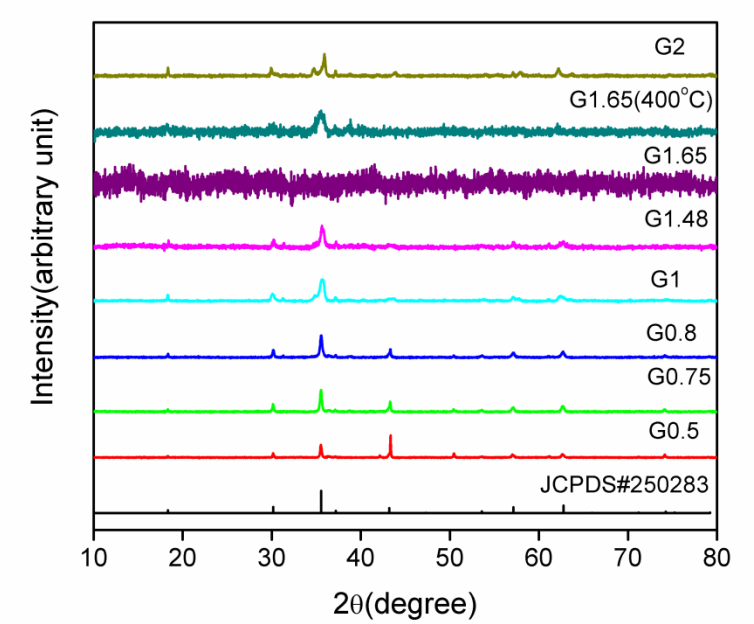

Figure 1: XRD patterns of Copper ferrite samples synthesized by autocombustion method. The metal to glycine ratio are indicated in the figure. Here G# represents glycine to metal ions ratio for a particluar sample. JCPDS(Joint Committee on Powder Diffraction Standards) -250283 represents the standard pattern for pure cubic phase of $CuFe_2O_4$ to compare with the observed XRD patterns.

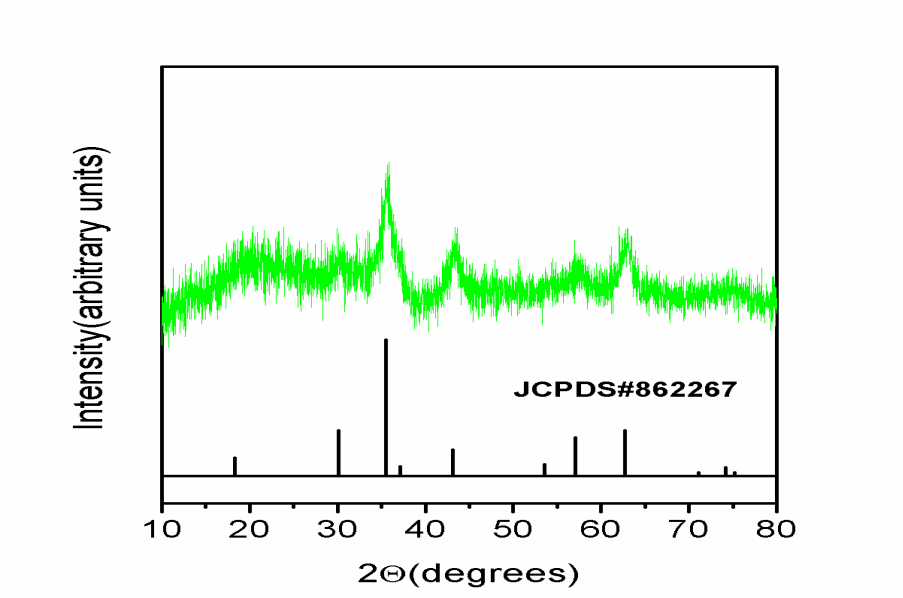

Figure 2: XRD patterns of $NiFe_2O_4$ sample synthesized by autocombustion method compared with the pure cubic phase of $NiFe_2O_4$. JCPDS(Joint Committee on Powder Diffraction Standards)#862267 represents the standard pattern for pure cubic phase of $NiFe_2O_4$.

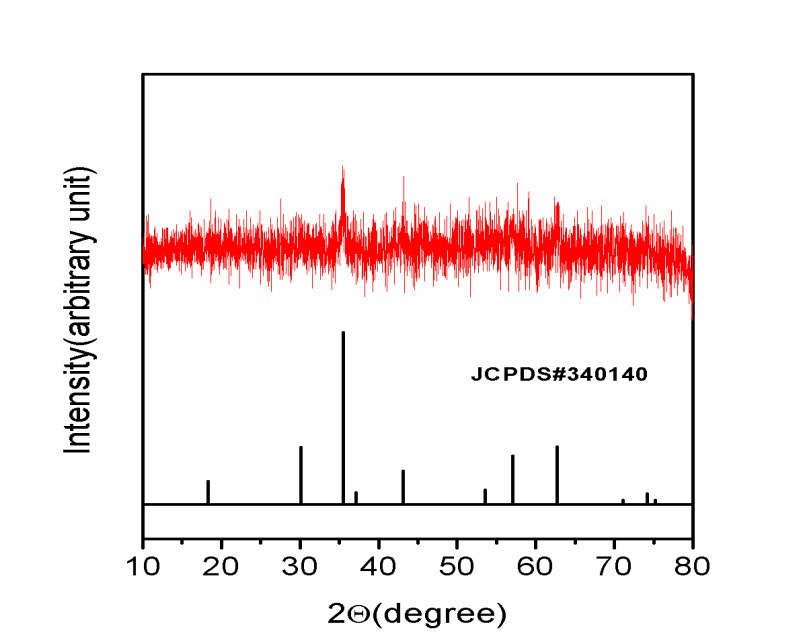

.

Figure 3: XRD patterns of $CrFe_2O_4$ sample synthesized by autocombustion method compared with the pure cubic phase of $CrFe_2O_4$. JCPDS(Joint Committee on Powder Diffraction Standards)#340140 represents the standard pattern for pure cubic phase of $CrFe_2O_4$.

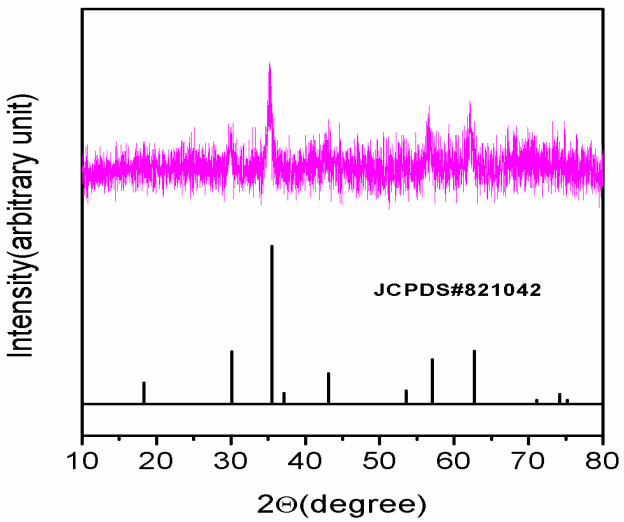

Figure 4: XRD patterns of $ZnFe_2O_4$ sample synthesized by autocombustion method compared with the pure cubic phase of $ZnFe_2O_4$. JCPDS(Joint Committee on Powder Diffraction Standards)#821042 represents the standard pattern for pure cubic phase of $ZnFe_2O_4$.

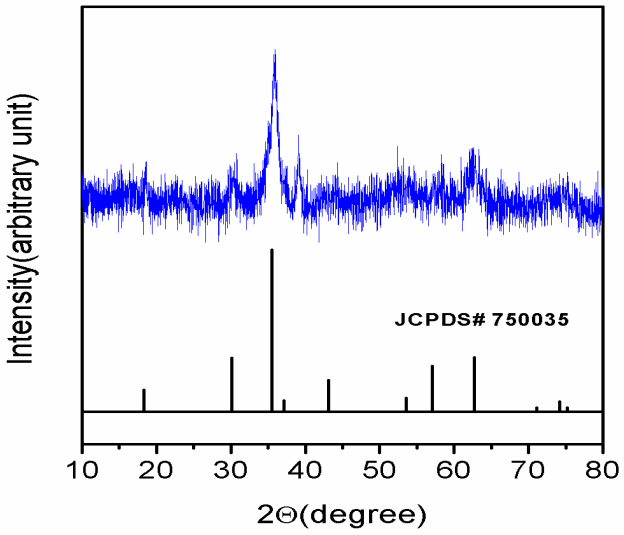

Figure 5: XRD patterns of $MnFe_2O_4$ sample synthesized by autocombustion method compared with the pure cubic phase of $MnFe_2O_4$. JCPDS(Joint Committee on Powder Diffraction Standards)#750035 represents the standard pattern for pure cubic phase of $MnFe_2O_4$.

3.4 Electrochemical characterization

Electrochemical characteristics were studied on a Biologic VMP 300 electrochemical workstation using a three electrode system composed of glassy carbon (working electrode), platinum electrode(counter electode) and Hg/HgO electrode(reference electrode).The working electrode was coated with a slurry obtained through following procedures. Electroactive material AFe_2O_4 (70wt%), carbon YP-50(15wt%) and PVDF binder(15wt%) were homogenously mixed in Isopropyl alcohol(IPA) to obtain a uniform slurry. This slurry was then coated on glassy carbon electrode. All the electrochemical measurements were performed in 1M KOH aqueous solution and the potential window taken are depicted in the corresponding figures of the electroactive material.

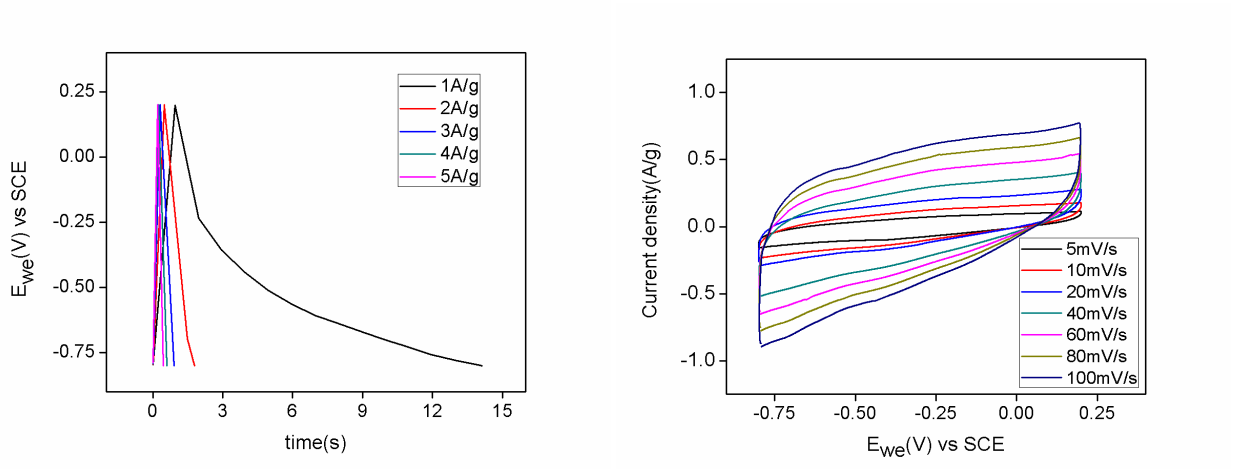

Figure6: Electrochemical measurements data from galvanostatic charge discharge technique and cyclic voltammetry technique for $CrFe_2O_4$ material.

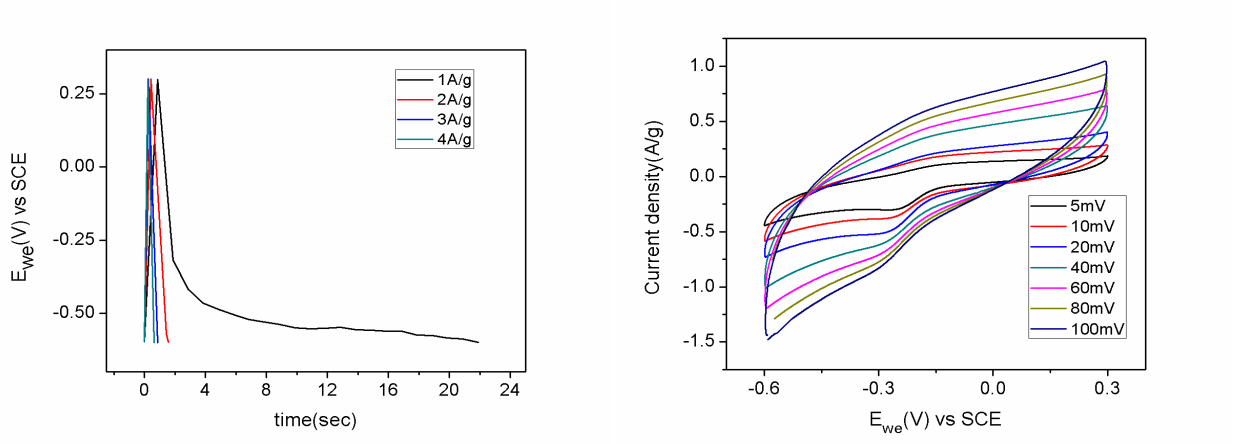

Figure7: Electrochemical measurements data from galvanostatic charge discharge technique and cyclic voltammetry technique for $ZnFe_2O_4$ material.

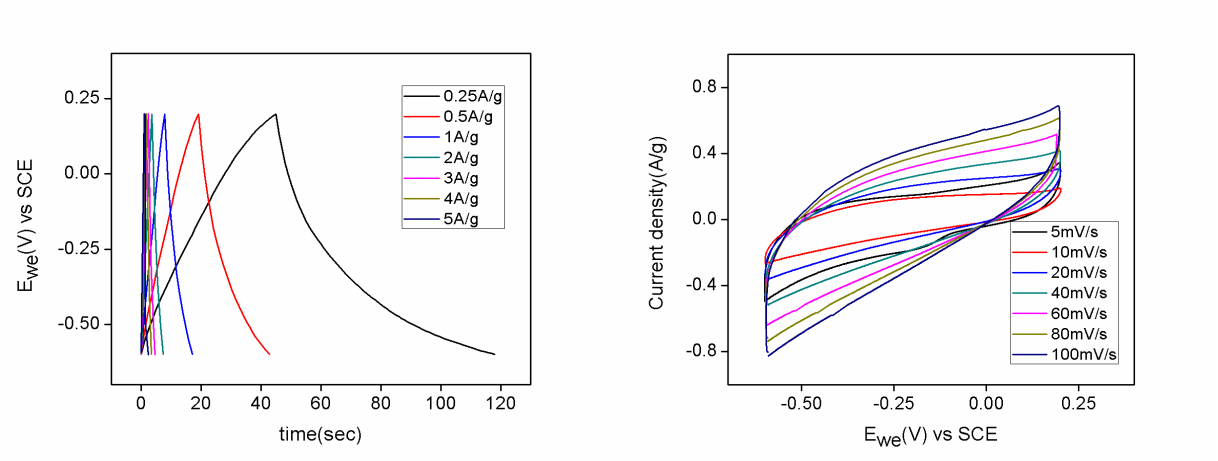

Figure 8: Electrochemical measurements data from galvanostatic charge discharge technique and cyclic voltammetry technique for $NiFe_2O_4$ material.

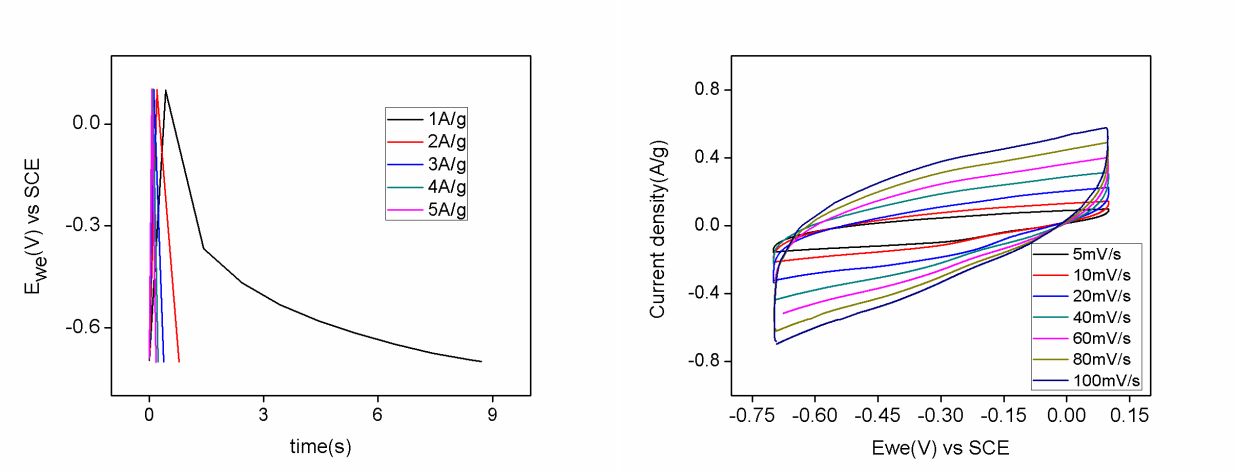

Figure 9: Electrochemical measurements data from galvanostatic charge discharge technique and cyclic voltammetry technique for $MnFe_2O_4$ materials.

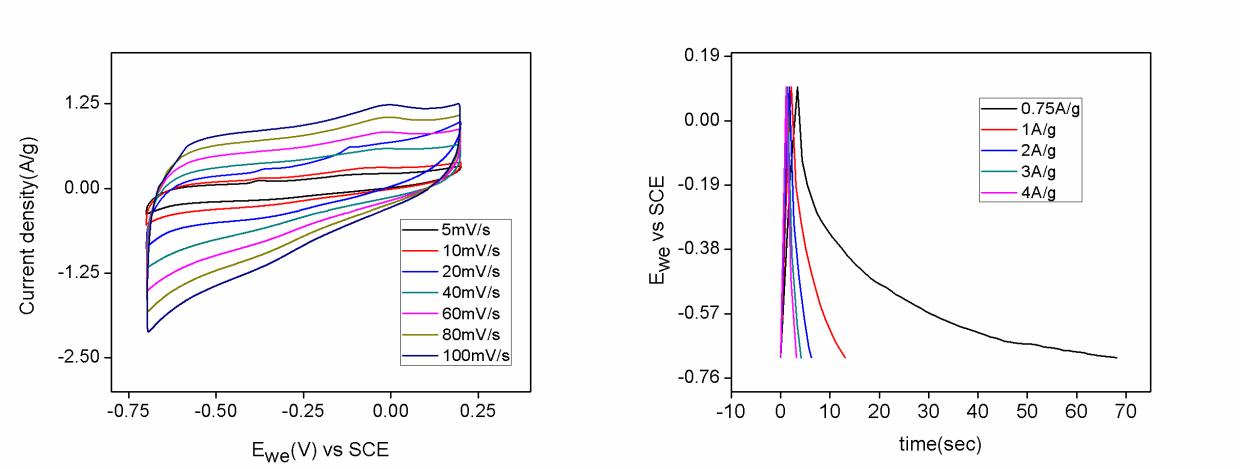

Figure 10: Electrochemical measurements data from galvanostatic charge discharge technique and cyclic voltammetry technique for $CuFe_2O_4$ material

3.5 Discussion

XRD patterns of spinel ferrites AFe_2O_4 ($CuFe_2O_4$, $NiFe_2O_4$, $CrFe_2O_4$, $ZnFe_2O_4$, $MnFe_2O_4$) synthesized using autocombustion methods shown in Figures 1, 2, 3, 4, 5 respectively. The obtained XRD patterns are compared with the respective standard patterns JCPDS(Joint Committee on Powder Diffraction Standards) for confirming the formation of the spinel phases.

In Figure 1, XRD patterns of Copper ferrite samples synthesized by autocombustion method are depicted. In case of $CuFe_2O_4$ synthesized by autocombustion, at lower glycine ratio (0.5) spinel phase is obtained. But, many impurities such as metallic Cu, CuO, Cu_2O and $CuFeO_2$ are identified. Increasing the glycine ratio is reducing the number of impurities and obtained the pure spinel phase with lesser impurities at the glycine ratio of 1.48. When we increase the glycine ratio more than 1.48, induces the formation of tetragonal phase. For example, copper ferrite synthesized at the glycine ratio of 2 results in the pure tetragonal phase with some impurities.

In Figure 2, 3, 4, 5 XRD patterns of $NiFe_2O_4$, $CrFe_2O_4$, $ZnFe_2O_4$, $MnFe_2O_4$ samples synthesized by autocombustion method are depicted. The glycine per metal ion ratio of 0.5 was taken for synthesis. The XRD patterns of the compounds match with pattern of respective pure cubic phase. This confirms the formation of spinel phase of these ferrite samples.

In Figure 6, 7, 8, 9, 10 graphs obtained from electrochemical measurements from cyclic voltammetry and galvanostatic charge discharge techniques of the synthesized spinel ferrites are shown. The measurements were carried out in 3 electrode system.

In Figure 6 graphs depicts curves obtained from cyclic voltammetry and galvanostatic charge discharge techniques when $CrFe_2O_4$ electroactive material is coated on working electrode. Specific capacitance is calculated using equation (1) and (2). Specific capacitance of 24F/g is calculated from cyclic voltammetry measurements at scan rate of 5mV/s and specific capacitance of 25 F/g is calculated from galvanostatic charge discharge measurements at a current density of 1 A/g.

In Figure 7 graphs depicts curves obtained from cyclic voltammetry and galvanostatic charge discharge techniques when $ZnFe_2O_4$ electroactive material is coated on working electrode. Specific capacitance of 16 F/g is calculated from cyclic voltammetry measurements at scan rate of 5mV/s and specific capacitance of 18 F/g is calculated from galvanostatic charge discharge measurements at a current density of 1 A/g.

In Figure 8 graphs depicts curves obtained from cyclic voltammetry and galvanostatic charge discharge techniques when $NiFe_2O_4$ electroactive material is coated on working electrode. Specific capacitance of 18 F/g is calculated from cyclic voltammetry measurements at scan rate of 5mV/s and specific capacitance of 15 F/g is calculated from galvanostatic charge discharge measurements at a current density of 0.25 A/g.

In Figure 9 graphs depicts curves obtained from cyclic voltammetry and galvanostatic charge discharge techniques when $MnFe_2O_4$ electroactive material is coated on working electrode. Specific capacitance of 22 F/g is calculated from cyclic voltammetry measurements at scan rate of 5mV/s and specific capacitance of 27 F/g is calculated from galvanostatic charge discharge measurements at a current density of 1 A/g.

In Figure 10 graphs depicts curves obtained from cyclic voltammetry and galvanostatic charge discharge techniques when $CuFe_2O_4$ electroactive material is coated on working electrode. Specific capacitance of 31 F/g is calculated from cyclic voltammetry measurements at scan rate of 5mV/s and specific capacitance of 36 F/g is calculated from galvanostatic charge discharge measurements at a current density of 0.5 A/g.

Table2: Divalent ion substituted nanosized spinel ferrites are shown with their crystallite size and observed Specific Capacitance values obtained from cyclic voltammetry technique and galvanostatic charge- discharge technique.

S.No.	Compound	Crystallite Size(nm)	Specific Capacitance (F/g) (from cyclic voltammetry technique)	Specific Capacitance(F/g)(from galvanostatic charge-discharge technique)
1	$CrFe_2O_4$	18	24	25
2	$ZnFe_2O_4$	17	16	18
3	$NiFe_2O_4$	20	18	15
4	$MnFe_2O_4$	22	22	27
5	$CuFe_2O_4$	25	31	36

3.6 Conclusion

The electrochemical studies of divalent ion substituted spinel ferrites shows that $CuFe_2O_4$ has highest specific capacitance among all which can be due to the presence of CuO like impurities. $NiFe_2O_4$ and $MnFe_2O_4$ shows comparatively lower specific capacitance values of 20 Farad per gram and 22 Farad per gram respectively. $CrFe_2O_4$ and $ZnFe_2O_4$ shows least specific capacitance values among all.

Chapter 4

Electrochemical studies of trivalent ion substituted spinel oxides

4.1 Introduction

In the present study, spinel oxides $NiFe_2O_4$, $NiAlFeO_4$, $NiAl_2O_4$ and $Li_{0.5}Fe_{2.5}O_4$ are synthesized by auto combustion method [17]. The replaced ion Al^{3+} does not exhibit multiple oxidation states while Fe^{3+} ion does. Thus induction of Al^{3+} will significantly affect the electrochemical characteristics from the $NiFe_2O_4$. In case of $Li_{0.5}Fe_{2.5}O_4$, quantity of Fe^{3+} is higher as compared to $NiFe_2O_4$, $NiAlFeO_4$ and $NiAl_2O_4$ .The objective of this study is that we will be able to infer role of Fe^{3+} ion in spinel ferrites ($NiFe_2O_4$, $NiAlFeO_4$, $NiAl_2O_4$ and $Li_{0.5}Fe_{2.5}O_4$).

4.2 Material synthesis

Autocombustion method is employed for the synthesis of nanostructured spinel oxides $NiFe_2O_4$, $NiAlFeO_4$, $NiAl_2O_4$ and $Li_{0.5}Fe_{2.5}O_4$. The Stoichiometric amounts of $Ni(NO_3)_2.3H_2O$, $Al(NO_3)_3.9H_2O$ and $Fe(NO_3)_3.9H_2O$ are dissolved for a required particular material with glycine(fuel) in minimum amount of distilled water in a beaker. Similariliy stoichiometric amounts of $Li(NO_3)_2.3H_2O$ and $Fe(NO_3)_3.9H_2O$ are dissolved with glycine(fuel) in minimum amount of distilled water in a beaker for preparation of $Li_{0.5}Fe_{2.5}O_4$ nanoparticles. The metal to glycine ratio of 0.5 is taken. The solution kept into a crystalline dish heated at 250^oC on a hot plate. After complete autocombustion ash is collected.

4.3 Material Characterization

In the present study, XRD patterns of the calcined and sintered powders were recorded on a PANalytical X'pert pro powder X-ray diffraction using Cu-K_α radiation with a wavelength of 1.5405 Å for $K_{\alpha1}$ and 1.5443 Å for $K_{\alpha2}$. The K_β component which is having a wavelength of 1.3922 Å was removed using Ni-β filter. The voltage and current applied for X-ray tube to generate the required wavelength were 30 mA and 40 kV, respectively and the sample was scanned in the 2θ range 10-80 degrees for 1Hour.

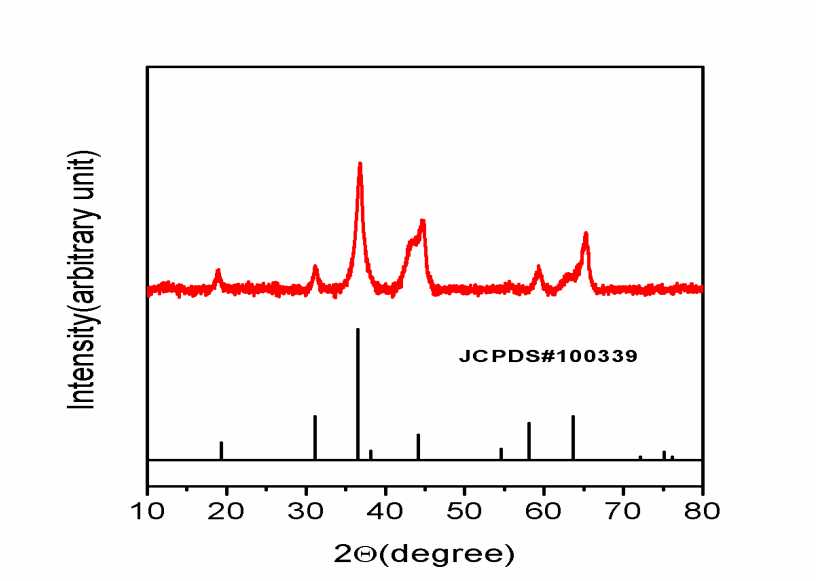

Figure 11: XRD patterns of $NiAl_2O_4$ sample synthesized by autocombustion method compared with the pure cubic phase. JCPDS(Joint Committee on Powder Diffraction Standards)#100339 represents the standard pattern for pure cubic phase of $NiAl_2O_4$.

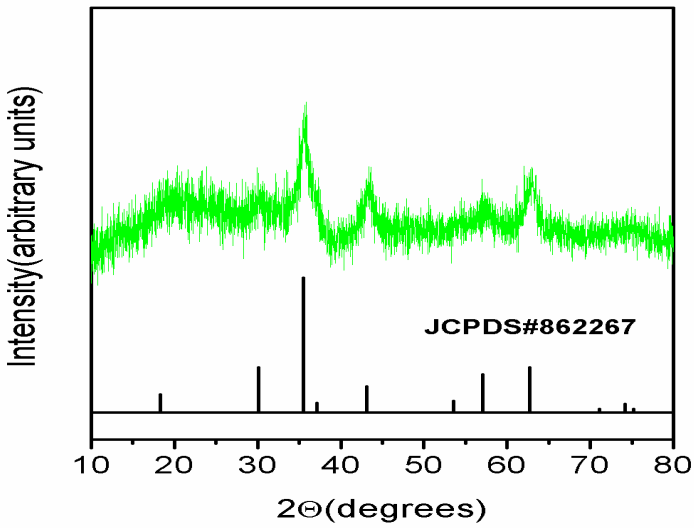

Figure 12: XRD patterns of $NiFe_2O_4$ sample synthesized by autocombustion method compared with its pure cubic phase. JCPDS(Joint Committee on Powder Diffraction Standards)#862267 represents the standard pattern for pure cubic phase of $NiFe_2O_4$.

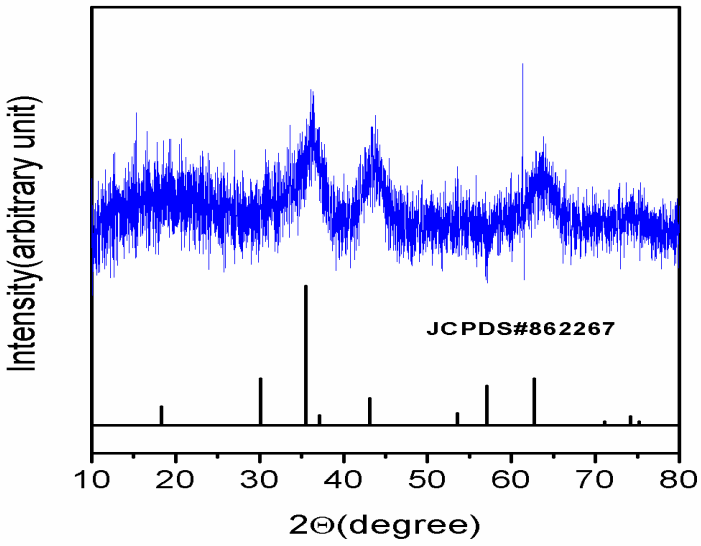

Figure 13: XRD patterns of $NiAlFeO_4$ sample synthesized by autocombustion method compared with the pure cubic phase. JCPDS(Joint Committee on Powder Diffraction Standards)#862267 represents the standard pattern for pure cubic phase of $NiFe_2O_4$. The peaks are slightly rightward shifted in observed pattern because of size difference between Al ion and Fe ion.

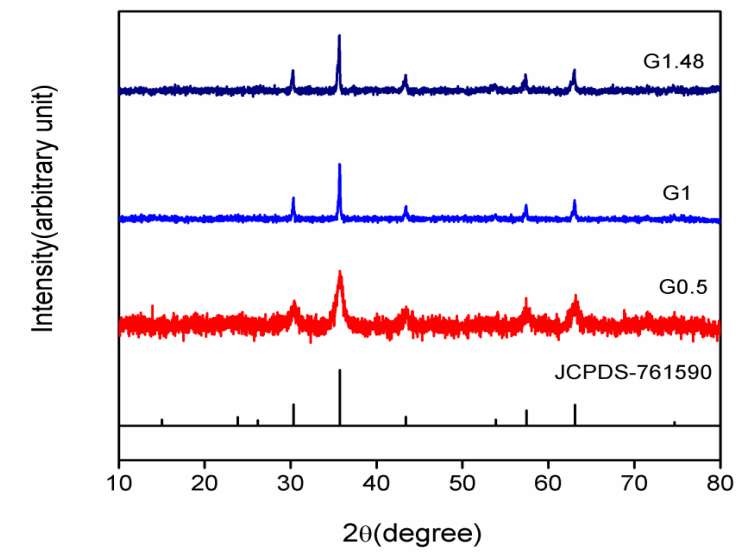

Figure1**4**: XRD patterns for Lithium Ferrites samples by autocombustion method. The metal to glycine ratio are indicated in the figure. Here G# represents metal to glycine ratio for a particluar sample. JCPDS(Joint Committee on Powder Diffraction Standards)-761590 represents the standard pattern for pure phase of $Li_{0.5}Fe_{2.5}O_4$.

4.4 Electrochemical characterization

Electrochemical characteristics were studied on a Biologic VMP 300 electrochemical workstation using a three electrode system composed of glassy carbon (working electrode), platinum electrode (counter electrode) and Hg-HgO electrode(reference electrode). The working electrode was coated with a slurry obtained through following procedures. Electroactive materials (70wt %), carbon YP-50(15wt %) and PVDF binder (15wt %) were homogenously mixed in Isopropyl alcohol (IPA) to obtain a uniform slurry. This slurry was then coated on glassy carbon electrode. All of the electrochemical measurements were performed in 1M KOH aqueous solution and potential window taken are depicted in the corresponding figures of the electroactive material.

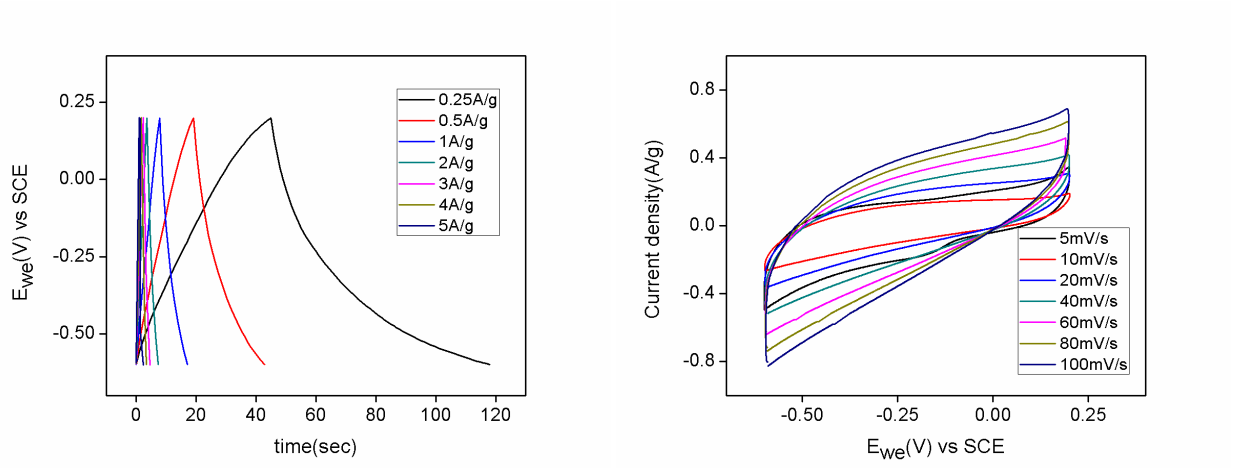

Figure 15: Electrochemical measurements data from galvanostatic charge discharge technique and cyclic voltammetry technique for $NiFe_2O_4$ material.

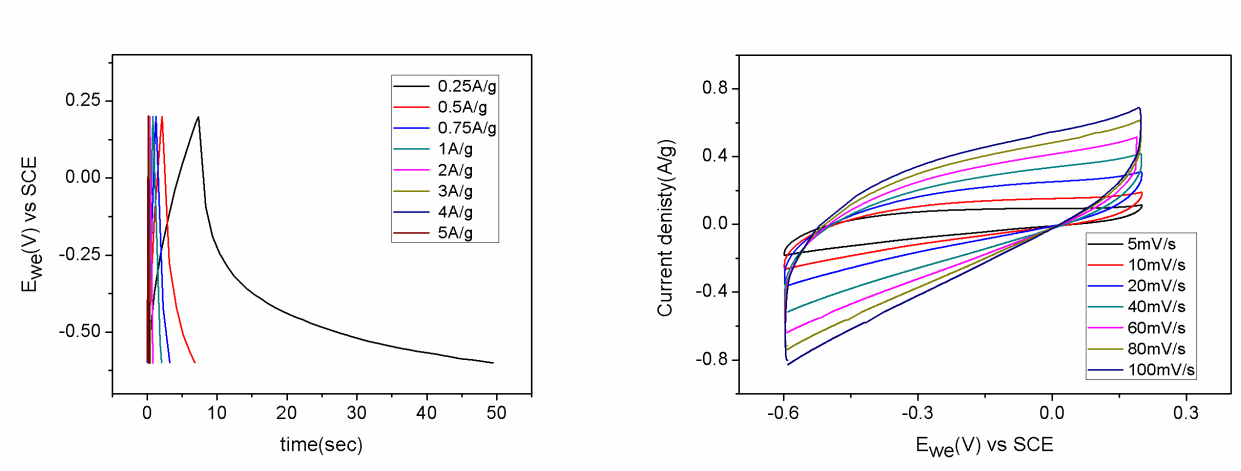

Figure 16: Electrochemical measurements data from galvanostatic charge discharge technique and cyclic voltammetry technique for $NiAlFeO_4$ material.

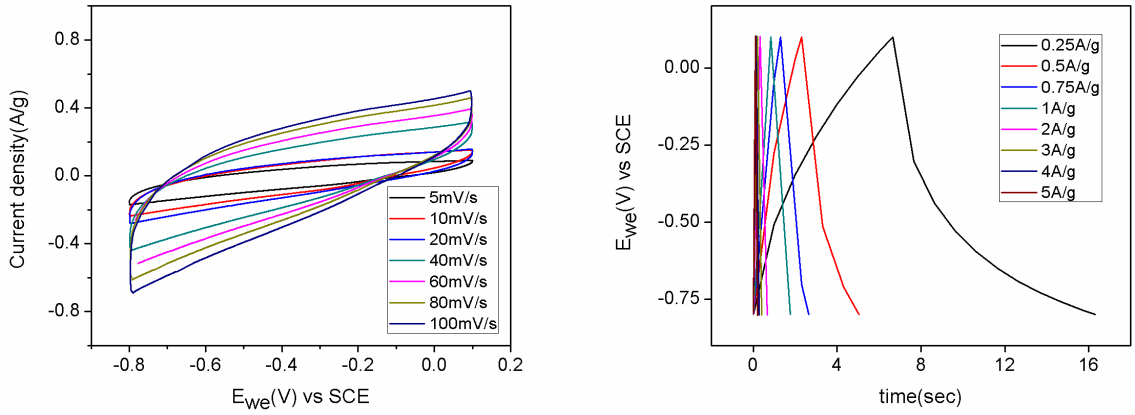

Figure 17: Electrochemical measurements data from galvanostatic charge discharge technique and cyclic voltammetry technique for $NiAl_2O_4$ material.

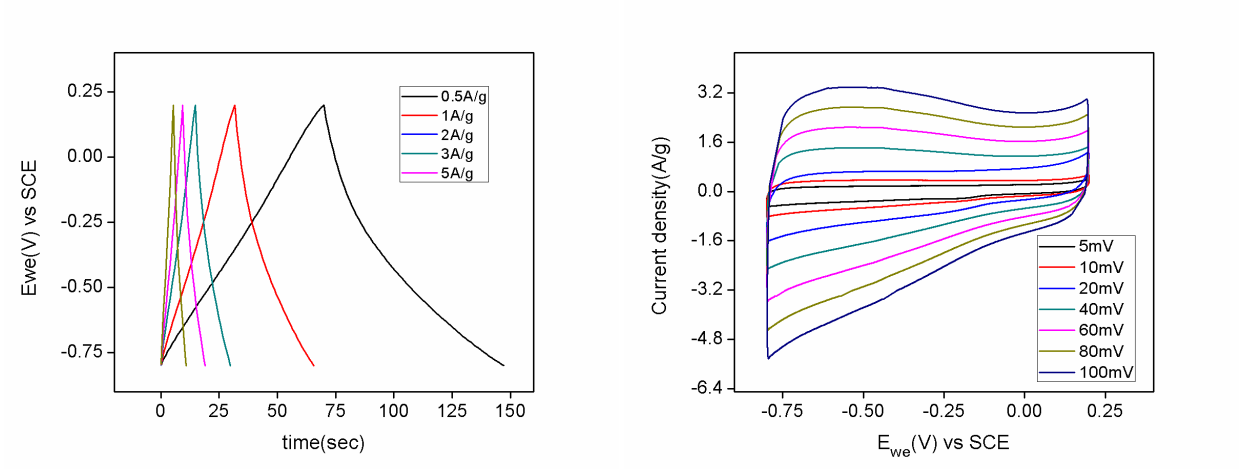

Figure 18: Electrochemical measurements data from galvanostatic charge discharge technique and cyclic voltammetry technique for $Li_{0.5}Fe_{2.5}O_4$ material.

4.5 Discussion

XRD patterns of spinel ferrites AFe_2O_4 ($NiAl_2O_4$, $NiFe_2O_4$, $NiAlFeO_4$) and $Li_{0.5}Fe_{2.5}O_4$ synthesized using autocombustion shown in Figure 11, 12, 13, 14. The obtained XRD patterns are compared with the respective "JCPDS(Joint Committee on Powder Diffraction Standards)" patterns for confirming the formation of the spinel phases.

The glycine per metal ion ratio of 0.5 for synthesis was taken. The XRD patterns of the compounds are matching with pattern of respective pure cubic phase. This confirms the formation of spinel phase of these ferrite samples.

In Figures 15, 16, 17 and 18, graphs obtained from electrochemical measurements from cyclic voltammetry and galvanostatic charge discharge techniques of the synthesized spinel ferrites are shown. The measurements were carried out in 3 electrode system.

In Figure 15, graphs depict curves obtained from cyclic voltammetry and galvanostatic charge discharge techniques when $NiFe_2O_4$ electroactive material is coated on working electrode. Specific capacitance is calculated using equation (1) and (2). Specific capacitance of 18 F/g is calculated from cyclic voltammetry measurements at scan rate of 5mV/s and specific capacitance of 15 F/g is calculated from galvanostatic charge discharge measurements at a current density of 0.25 A/g.

In Figure 16, graphs depict curves obtained from cyclic voltammetry and galvanostatic charge discharge techniques when $NiAlFeO_4$ electroactive material is coated on working electrode. Specific capacitance of 10 F/g is calculated from cyclic voltammetry measurements at scan rate of 5mV/s and specific capacitance of 9 F/g is calculated from galvanostatic charge discharge measurements at a current density of 0.25 A/g.

In Figure 17, graphs depict curves obtained from cyclic voltammetry and galvanostatic charge discharge techniques when $NiAl_2O_4$ electroactive material is coated on working electrode. Specific capacitance of 6 F/g is calculated from cyclic voltammetry measurements at scan rate of 5mV/s and specific capacitance of 5 F/g is calculated from galvanostatic charge discharge measurements at a current density of 0.25 A/g.

In Figure 18, graphs depict curves obtained from cyclic voltammetry and galvanostatic charge discharge techniques when $Li_{0.5}Fe_{2.5}O_4$ electroactive material is coated on working electrode. Specific capacitance of 32 F/g is calculated from cyclic voltammetry measurements at scan rate of 5mV/s and specific capacitance of 52 F/g is calculated from galvanostatic charge discharge measurements at a current density of 0.5 A/g.

Table3: Trivalent ion substituted nanosized spinel ferrites are shown with their crystallite size and observed Specific Capacitance values obtained from cyclic voltammetry technique and galvanostatic charge- discharge technique.

S.No.	Compound	Crystallite Size(nm)	Specific Capacitance(F/g)(from cyclic voltammetry technique)	Specific Capacitance(F/g)(from galvanostatic charge-discharge technique)
1	$NiFe_2O_4$	20	18	15
2	$NiAlFeO_4$	23	10	9
3	$NiAl_2O_4$	27	6	5
4	$Li_{0.5}Fe_{2.5}O_4$	10	32	52

4.6 Conclusion

The electrochemical studies of trivalent ion substituted spinel ferrites shows that $Li_{0.5}Fe_{2.5}O_4$ has highest specific capacitance amongst all due to the higher amount Fe^{3+} ion. Followed by $Li_{0.5}Fe_{2.5}O_4$, $NiFe_2O_4$ shows higher specifc capacitance compared to $NiAlFeO_4$ and $NiAl_2O_4$. The decrease in specific capacitance value of $NiAlFeO_4$ and $NiAl_2O_4$ as shown in Table 2 can be attributed to the fact that Al3+ ion doesn't exhibit multiple oxidation state while Fe^{3+} does. Further, it can be inferred that Fe3+ significantly plays larger role as compared to the divalent ions studied in previous chapter.

Chapter 5

Conclusions and Future perspective

5.1 Conclusion

Spinel ferrites ($ZnFe_2O_4$, $MnFe_2O_4$, $NiFe_2O_4$, $CrFe_2O_4$, $CuFe_2O_4$, $NiAlFeO_4$, $NiAl_2O_4$, $Li_{0.5}Fe_{2.5}O_4$) have been synthesized by autocombustion method. We obtained spinel phase of $CuFe_2O_4$ with some inpurities whereas the rest of the spinel phase material are of pure phase. The phase purity is investigated using data collected from XRD technique.

In case of spinel ferrites $ZnFe_2O_4$, $MnFe_2O_4$, $NiFe_2O_4$, $CrFe_2O_4$ and $CuFe_2O_4$ where Divalent ion is substituted by another metal ion, the specific capacitance value changes signifying the role of divalent metal ion.

In case of spinel ferrites $NiFe_2O_4$, $NiAlFeO_4$ and $NiAl_2O_4$ where trivalent metal ions are substituted, the decrease in specific capacitance value by decreasing the amount of Fe^{3+} ion resonates with the the fact that Fe^{3+} ion is forming a redox couple. Also in case of $Li_{0.5}Fe_{2.5}O_4$ where Fe^{3+} ion content is increased per divalent ion the specific capacitance is higher signifying the role of Fe^{3+} exhibiting multiple oxidation states during electrochemical measurements.

The metal ions in the spinel ferrite materials are not only the contributing factor affecting electrochemical measurements. Morphology of the material, size of the nanoparticles and porosity of material significantly affect the specific capacitance measurements. The particle size of the synthesized materials calculated from Scherrer's formula lies between 10-30nm.Therefore in these cases, low porosity (means higher surface area) and morphology can be held accountable for observed low specific capacitance values.

5.2 Future Perspective

- Obtaining pure phase of spinel ferrites is necessary to use them as potential candidate of supercapacitor applications.
- Glycine is used as fuel in the present synthesis of spinel ferrites while use of other fuels like urea , citic acid, tartaric acid etc. can be explored.
- The particle size, porosity and morphology of the synthesized materials significantly affect the electrochemical measurements therefore other methods of synthesis can be explored.
- Electrochemical measurement studies can be performed on Composite materials (formed by substituting the divalent and trivalent ions in different stoichiometric amount with different metal ions).

REFERENCES

1. Simon, Patrice, and Yury Gogotsi. "Materials for electrochemical capacitors." *Nanoscience And Technology: A Collection of Reviews from Nature Journals*. 2010. 320-329.

2. Mathew, Daliya S., and Ruey-Shin Juang. "An overview of the structure and magnetism of spinel ferrite nanoparticles and their synthesis in microemulsions." *Chemical engineering journal* 129.1-3 (2007): 51-65.

3. Sugimoto, Mitsuo. "The past, present, and future of ferrites." *Journal of the American Ceramic Society* 82.2 (1999): 269-280.

4. Sickafus, Kurt E., John M. Wills, and Norman W. Grimes. "Structure of spinel." *Journal of the American Ceramic Society*82.12 (1999): 3279-3292.

5. Bragg, William Henry. "XXX. The structure of the spinel group of crystals." *The London, Edinburgh, and Dublin Philosophical Magazine and Journal of Science* 30.176 (1915): 305-315.

6. http://hegegy.web.elte.hu/Anyagtudomány-tankönyv.

   Online available at website http://hegegy.web.elte.hu/Anyagtudomány-tankönyv.

7. Snelling, Eric Charles. *Soft ferrites: properties and applications*. London: Iliffe Books, 1969.

8. Frackowiak, Elzbieta. "Carbon materials for supercapacitor application." *Physical chemistry chemical physics* 9.15 (2007): 1774-1785.

9. Petcharoen, K., and A. Sirivat. "Synthesis and characterization of magnetite nanoparticles via the chemical co-precipitation method." *Materials Science and Engineering: B* 177.5 (2012): 421-427.

10. https://en.wikipedia.org/wiki/Supercapacitor.

    Online available at website https://en.wikipedia.org/wiki/Supercapacitor

11. Sutka, Andris, and Gundars Mezinskis. "Sol-gel auto-combustion synthesis of spinel-type ferrite nanomaterials." *Frontiers of Materials Science* 6.2 (2012): 128-141.

12. Milovanovic, Nesa, and Rui Chen. "A review of experimental and simulation studies on controlled auto-ignition combustion." (2001).

13. Klug, Harold P., and Leroy E. Alexander. "X-ray diffraction procedures: for polycrystalline and amorphous materials." *X-Ray Diffraction Procedures: For Polycrystalline and Amorphous Materials, 2nd Edition, by Harold P. Klug, Leroy E. Alexander, pp. 992. ISBN 0-471-49369-4. Wiley-VCH, May 1974.* (1974): 992.

14. Roy, P. K., and J. Bera. "Characterization of nanocrystalline NiCuZn ferrite powders synthesized by sol–gel auto-combustion method." *Journal of materials processing technology* 197.1-3 (2008): 279-283.

15. Biswas, Sanjib, and Lawrence T. Drzal. "Multilayered nano-architecture of variable sized graphene nanosheets for enhanced supercapacitor electrode performance." *ACS applied materials & interfaces* 2.8 (2010): 2293-2300.

16. Allagui, Anis, et al. "Reevaluation of performance of electric double-layer capacitors from constant-current charge/discharge and cyclic voltammetry." Scientific reports 6 (2016): 38568.

17. Patterson, A. L. "The Scherrer formula for X-ray particle size determination." *Physical review* 56.10 (1939): 978.

18. Wei, Chao, et al. "Valence change ability and geometrical occupation of substitution cations determine the pseudocapacitance of spinel ferrite XFe2O4 (X= Mn, Co, Ni, Fe)." *Chemistry of Materials* 28.12 (2016): 4129-4133.